

FSR HW4

Gianmarco Iodice P38000260 <https://github.com/gianmarcoiodice/FSR-HW4>

June 2025

1. Describe the buoyancy effect and why it is considered in underwater robotics while it is neglected in aerial robotics.

When a rigid body is submerged in a fluid under the effect of gravity the buoyancy must be considered. The buoyancy is a hydrostatic effect since it is not function of the relative movement between the body and the fluid. This effect is strongly related to the density of the fluid: if the fluid's density is lower than that of the object, the object tends to sink; otherwise, it tends to float. Therefore, the outcome depends on the balance between the buoyancy force and gravity. In aerial robotics, the buoyancy effect is negligible because the density of air is extremely low compared to that of the robot. As a result, the buoyant force is negligible when compared to other forces such as gravity. Its effect is so small that it can be safely ignored without significantly affecting the system's dynamics. In underwater robotics the density of the robot and that of the water are comparable, so the buoyancy effect must be considered. Define: $\bar{g} = [0 \ 0 \ g]^T \in \mathbb{R}^3$, $g \in \mathbb{R}$ the gravity acceleration, $\Delta \in \mathbb{R}$ the volume of the body, $m \in \mathbb{R}$ the mass of the body, $\rho \in \mathbb{R}$ the density of the water. The buoyancy is $b = \rho\Delta\|\bar{g}\|$

The buoyancy force acts at the center of buoyancy, $r_b^b \in \mathbb{R}^3$, and it is equal to

$$f_b^b = -R_b^T \begin{bmatrix} 0 \\ 0 \\ b \end{bmatrix} = -R_b^T \begin{bmatrix} 0 \\ 0 \\ \rho\Delta g \end{bmatrix}$$

The negative sign arises from the fact that the z-axis is oriented downwards. Since we consider the gravitational force as positive in this direction, the buoyant force acts in the opposite direction and therefore carries a negative sign. Typically, we assume the center of mass is where the gravity force is applied. The center of buoyancy is determined by the geometry of the submerged volume of the body often, these two centers don't coincide. When designing an underwater robot, one important requirement is to align the center of gravity and the center of buoyancy along the same vertical axis. If there is even a small displacement between these two centers along the x or y axes, it will generate an induced torque, which can cause undesired rotational motion or resistance effects.

2. Briefly justify whether the following expressions are true or false.

1. The added mass effect considers an additional load to the structure. **FALSE**

When a rigid body through a fluid, the surrounding fluid particles are accelerated as a result of its motion. According to Newton's second law ($F=ma$), any acceleration implies the presence of a force. In this case, however, the force responsible for the acceleration of the fluid particles is not directly applied by an external source; rather, it arises due to the interaction with the moving robot. This apparent force can be interpreted as a virtual force, induced by the robot's motion, and represents a reaction of the fluid to the disturbance introduced by the robot itself. The fluid exerts a reaction force which is equal in magnitude and opposite in direction, this reaction force is called the added mass contribution. This phenomenon is closely related to the inertia of the system the body behaves as if it has more mass than it actually does although the physical mass of the object remains unchanged. In fact, to initiate and maintain motion, the body must exert a greater force, as if it were responding to an increased mass. The expression is **FALSE** since the robot does not actually gain additional mass; this effect only appears during motion and is absent under static conditions so the added mass effect doesn't consider an additional load to the structure.

2. The added mass effect is considered in underwater robotics since the density of the underwater robot is comparable to the density of the water. **TRUE**

The added mass effect is influenced by the fluid's density, since the robot must accelerate a certain amount of fluid as it moves. This effect has been neglected for the legged robots, because the air density is much

lighter than the density of the moving mechanical system. In underwater applications, instead, the density of the water is comparable with the density of the robot. This effect also depends on body's geometry, as it influences the volume of fluid that is set into motion during acceleration.

3. The damping effect helps in the stability analysis. **TRUE**

The viscosity of the surrounding fluid leads to the presence of dissipative forces, such as drag and lift, acting on the body of underwater vehicles. A common modeling simplification is to consider only quadratic damping terms, which are grouped into a damping matrix $D_{RB} \in \mathbb{R}^{6 \times 6}$. This matrix is assumed to be positive definite and its coefficients are often treated as constant, which also facilitates stability analysis. The viscous effects are typically modeled as the combination of two main components: the drag force, which acts parallel to the relative velocity between the body and the fluid, and the lift force, which acts orthogonally to the drag. These forces are generally assumed to act at the center of mass of the vehicle. The expression is **TRUE** since the damping effect helps in stability analysis, as it acts as a resisting force that counteracts the motion of the underwater robot. This resistance simplifies the control of the robot's dynamics and plays a critical role in maintaining its stability.

In Lyapunov-based stability analysis, damping terms contribute to making the time derivative of the Lyapunov function more negative. This behavior leads to faster convergence of the system's state toward the desired equilibrium. A clear example of this can be seen in the expression used in a model-based controller structured in a mixed Earth/Vehicle-fixed frame (refer to *Underwater Robots*, G. Antonelli, p.72):

$$\dot{V} = -s_v^T(K_D + D_{RB})s_v - k_p\lambda_p\tilde{p}_b^T\tilde{p}_b - k_o\epsilon^T\epsilon \leq 0$$

In this equation, the matrix D_{RB} contributes to making \dot{V} more negative, reinforcing its negative semi-definiteness and thereby enhancing the overall stability of the system.

4. The ocean current is usually considered as constant, and it is better to refer it with respect to the body frame. **FALSE**

Just like in the air where we have wind, which is usually neglected, in the ocean and underwater you have to consider ocean currents. These currents are quite persistent compared to the state of wind. If you leave something in the water, you will notice that it starts to lift or move due to the influence of the currents. Usually the Ocean current is expressed in the world frame and it is constant and irrotational:

$$\mathbf{v}_c = \begin{bmatrix} v_{c,x} \\ v_{c,y} \\ v_{c,z} \\ 0 \\ 0 \\ 0 \end{bmatrix} \in \mathbb{R}^6, \quad \dot{\mathbf{v}}_c = \mathbf{0}_6$$

The expression is **FALSE** since if the ocean currents are expressed in the body frame of the UUV, they become time-varying due to the vehicle's motion through the water. This time dependence introduces complexity in developing a control law for the UUV, as the disturbance is no longer constant, making it more challenging to manage.

The related effect can be added to the dynamic model of a rigid body moving in a fluid simply considering the relative velocity in the body-fixed frame

$$\mathbf{v}_r = \begin{bmatrix} \dot{\mathbf{p}}_b^b \\ \omega_b^b \end{bmatrix} - R_b^T \mathbf{v}_c$$

where $\dot{\mathbf{p}}_b^b$ is the linear velocity of robot with respect the world frame expressed in the body frame, ω_b^b is the angular velocity of robot with respect the world frame expressed in the body frame, \mathbf{v}_c is the ocean current velocity in the world frame and R_b is the rotation matrix. Given that expressing the ocean current in the UUV's body frame introduces time-dependent variability which in turn complicates control design.

3. Consider the Matlab files within the quadruped_simulation.zip file. Within this folder, the main file to run is MAIN.m. The code generates an animation and plots showing the robot's

position, velocity, and z-component of the ground reaction forces. In this main file, there is a flag to allow video recording (`flag_movie`) that you can attach as an external reference or in the zip file you will submit. You must:

- Implement the quadratic function using the QP solver `qpSWIFT` located within the folder (refer to the instructions starting from line 68 in the file `MAIN.m`);
- Modify parameters in the main file, such as the gait and desired velocity, or adjust some physical parameters in `get_params.m`, such as the friction coefficient and mass of the robot. Execute the simulation and present the plots you find most interesting: you should analyze them to see how they change with different gaits and parameters and comment on them.

The desired joint accelerations \ddot{q}_j^* and the desired ground reaction forces f_{gr}^* are obtained as the output of a whole-body controller. A whole-body controller decouples motion planning from control execution. In the block diagrams of the control system, it is possible to identify several key components. One of them is the Trajectory Generator, which computes the desired trajectory for the Center of Mass (CoM). Another important component is the Foot Scheduler, which plans the contact schedule based on the desired gait. For a quadruped robot, different gaits can be realized using two stance legs, enabling highly dynamic motions. These include the *trot*, where diagonal leg pairs move together; the *pace*, where lateral legs move in coordination; and the *bound*, where front and rear legs move in pairs. The Motion Planner continuously replans the motion to follow the desired trajectory. It also computes the CoM reference based on the Zero Moment Point (ZMP) criterion, ensuring that the robot maintains balance. Based on this reference, the Wrench Reference Generator computes the desired wrench (i.e., force and torque) to be applied to the CoM. This wrench must be realized through the application of appropriate ground reaction forces, which are generated by the controller. The desired joint accelerations and ground reaction forces are obtained by solving a quadratic optimization problem.

$$\text{minimize } f(\zeta) \quad \text{subject to} \quad A\zeta = b, \quad D\zeta \leq c.$$

The cost function is based on the fact that I want to follow as the possible the wrench reference. This optimization considers several constraints to ensure the physical feasibility and effectiveness of the solution. These constraints include dynamic consistency, system should follow model dynamic that I derived from my system; non-sliding contact conditions, in order that the stance feet no sliding; torque limits; and swing leg tasks, follow exactly more or less the motion. The quadratic optimization problem is solved using the function `qpSWIFT`. Which takes as input a set of matrices that encode both the objective function and the associated constraints to solve the constrained optimization problem.

This section presents the robot's possible gaits and the corresponding simulations, obtained by varying parameters in the parameter file. The desired velocity was also adjusted in the main script.

Trot gait: is typically adopted at moderate speeds, offering a balance between energy efficiency and dynamic stability. It is a diagonal gait, meaning that the robot moves its front-left and rear-right limbs together, followed by the opposite pair. This pattern creates a symmetrical and rhythmic motion that minimizes vertical body oscillations and supports efficient forward progression. The trot gait is frequently chosen for tasks requiring stable, predictable motion across flat or mildly uneven terrain.

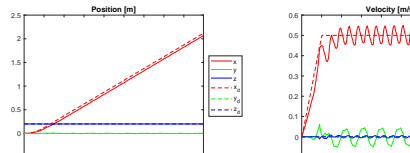


Figure 1: Trot gait $m = 5.5\text{Kg}$ $\mu=1$ $v_{des} = [0.5;0]\text{m/s}$

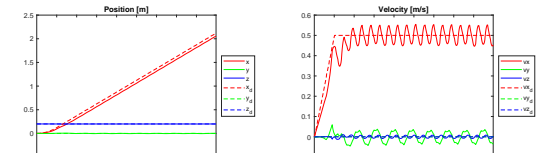
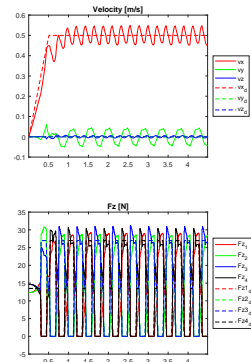


Figure 2: Trot gait $m = 8\text{Kg}$ $\mu=1$ $v_{des} = [0.5;0]\text{m/s}$

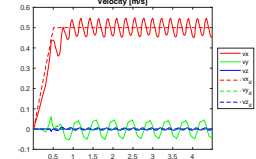
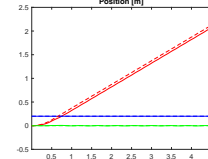
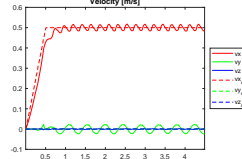
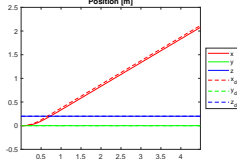


Figure 3: Trot gait $m = 1\text{Kg}$ $\mu=1$ $v_{des} = [0.5;0]\text{m/s}$

Figure 4: Trot gait $m = 5.5\text{Kg}$ $\mu=0.4$ $v_{des} = [0.5;0]\text{m/s}$

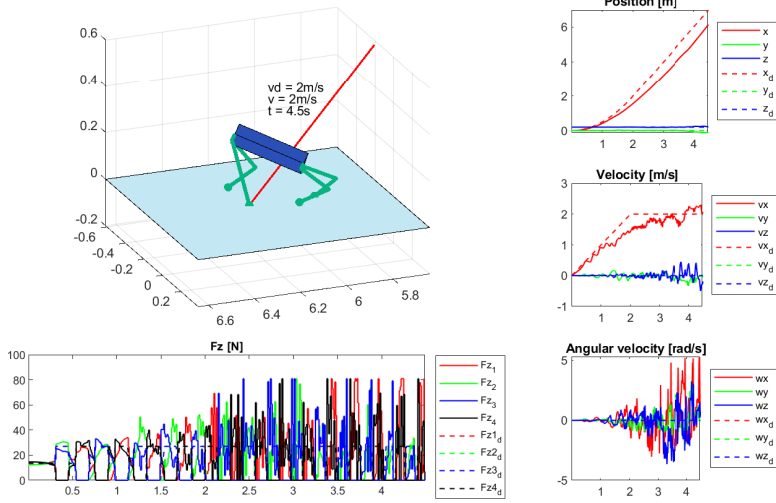


Figure 5: Trot gait $m = 5.5\text{Kg}$ $\mu=1$ $v_{des} = [2;0]\text{m/s}$

Using the parameters ($m = 5.5 \text{ kg}$, $\mu = 1$, $v_{des} = [0.5;0]\text{m/s}$), it is evident that the robot successfully tracks the position reference. The ground reaction forces along the z-axis remain moderate, with a maximum peak of 30 N. The velocity graph shows that the robot efficiently reaches the desired speed and maintains a stable, cyclic gait. The oscillations observed in the x-axis velocity are consistent with periodic leg movements and do not indicate any significant instability. The near-zero velocities along the y and z axes confirm that the robot maintains good lateral and vertical stability while moving primarily in the forward direction. By modifying the mass, it is possible to observe changes in the ground reaction forces: they increase, reaching peaks close to 45N for $m = 8\text{kg}$, and decrease to a maximum value of around 6N for $m = 1\text{kg}$. This indicates that the slipping effect is reduced with lower mass. As the speed increases ($v_{des} = [2;0]\text{m/s}$), the position error tends to grow due to the more dynamic nature of the gait. In such conditions, it becomes more challenging for the robot to accurately track the position and velocity references while simultaneously maintaining body stability. Previous simulations used a friction coefficient of $\mu = 1$, which is relatively high. Additional tests with an even higher value ($\mu = 2$), though difficult to replicate in real-world conditions, demonstrated that increased friction provides greater stability margins in the robot's gait. With higher friction, the robot is able to maintain stable locomotion at higher speeds without its gait deteriorating. Conversely, as shown in the graph for $\mu = 0.4$, lowering the coefficient of friction significantly impacts the robot's ability to stay balanced. The reduced ground traction makes it more difficult to maintain equilibrium, especially during fast or dynamic movements. This results in increased position and velocity errors, greater deviation from the reference trajectory, and a higher risk of slipping (**This observation holds true for the following gaits**). For this gait with $\mu = 0.4$ and $v_{des} = [0.5;0]\text{m/s}$, the robot performs well, maintaining a fairly stable gait with only a small delay.

Bound Gait: is a high-speed, asymmetrical locomotion pattern the forelimbs move together as a pair, followed by a synchronized movement of the hindlimbs, creating a distinct flight phase between the two

contacts. Unlike the trot, which maintains continuous ground contact with alternating diagonal limbs, the bound gait includes extended aerial phases and large ground reaction forces, making it suitable for fast and agile movement. The bound gait is often implemented when the goal is maximum speed, agile maneuvering, or clearance over gaps or rough terrain. However, it presents significant challenges in terms of stability, control, and actuation, due to the dynamic nature of the motion and the brief contact periods with the ground. (To change the desired velocity, it was necessary to modify the script fcnFsmBound, where the desired velocity was being overwritten.)

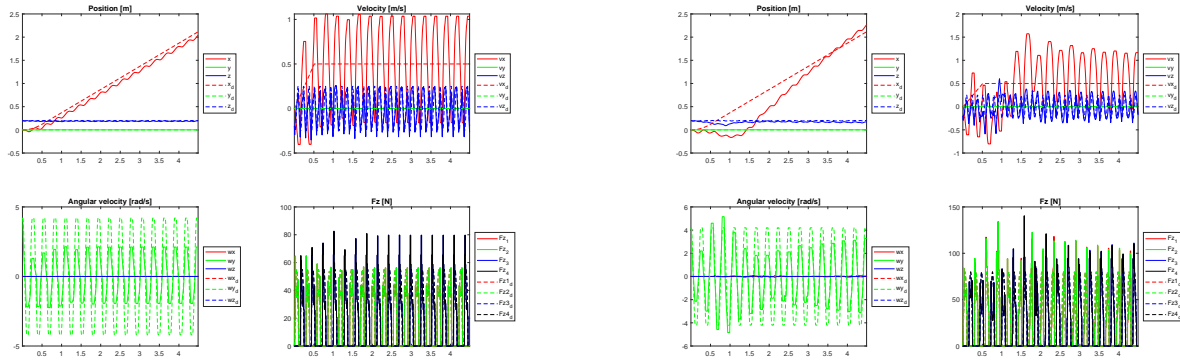


Figure 6: Bound gait $m = 5.5\text{Kg}$ $\mu=1$ $v_{des} = [0.5;0]\text{m/s}$

Figure 7: Bound gait $m = 8\text{Kg}$ $\mu=1$ $v_{des} = [0.5;0]\text{m/s}$

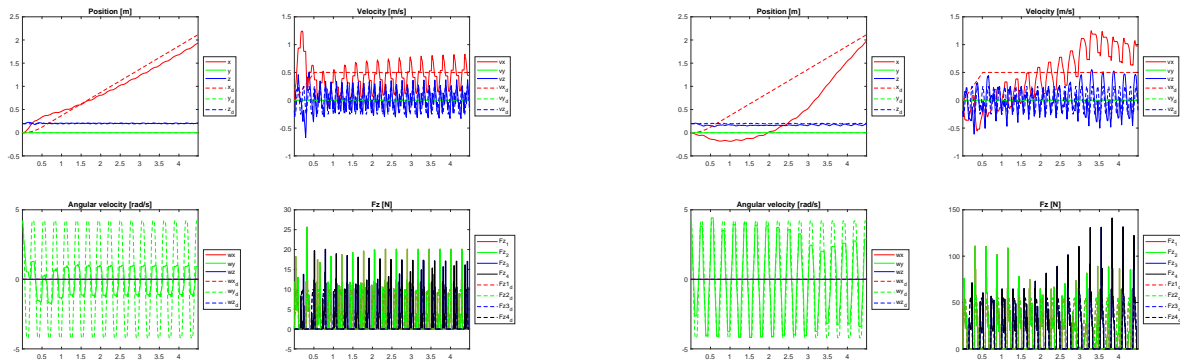


Figure 8: Bound gait $m = 1\text{Kg}$ $\mu=1$ $v_{des} = [0.5;0]\text{m/s}$

Figure 9: Bound gait $m = 5.5\text{Kg}$ $\mu=0.4$ $v_{des} = [0.5;0]\text{m/s}$

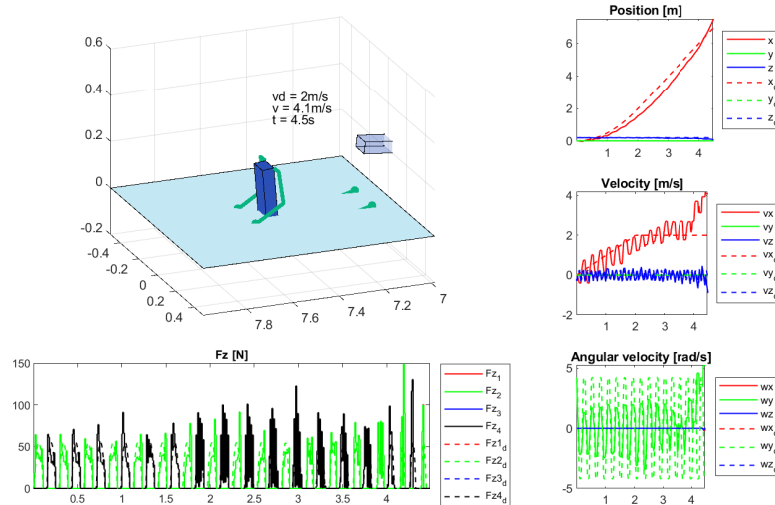


Figure 10: Bound gait $m = 5.5\text{Kg}$ $\mu=1$ $v_{des} = [2;0]\text{m/s}$

The ground reaction forces observed during this gait are significantly higher than those recorded in the trot gait , reaching around 80 N (with $m=5.5\text{kg}$, $\mu=1$ and $v_{des} = [0.5;0]\text{m/s}$. In addition, the position error is noticeably greater compared to the trot simulation. When the robot's mass is reduced (1 kg), the ground reaction forces decrease to approximately 25 N, yet this change does not result in improved stability. Conversely, increasing the mass to about 8 kg the initial position error is significantly higher compared to both the 1Kg and 5.5Kg cases, suggesting that the system struggles to maintain proper control from the onset. As for speed variations, the robot is generally capable of maintaining its trajectory even at higher speeds, with only a slight increase in position error and ground reaction forces. As speed increases, the robot is generally able to follow its trajectory without significant difficulty. The outcomes remain comparable to those observed under standard conditions, with a rise in ground reaction forces.Unlike other gaits, this one allows the robot to sustain relatively high speeds without immediately deviating from its intended path.However, reducing the coefficient of friction introduces considerable instability. The robot struggles to maintain effective ground contact, resulting in noticeable peaks in ground reaction forces that indicate slipping and an increased risk of losing balance. These peaks can reach very high values, approximately 145 N, highlighting the severity of the loss of traction.

Pacing Gait: is a type of symmetrical, lateral gait in which the limbs on the same side of the body (e.g., front-left and rear-left) move forward simultaneously, followed by the opposite side.This is in contrast to the trot gait, where diagonally opposite limbs move together.It offers advantages in terms of reduced body oscillation and greater lateral stability at low to moderate speeds.The pacing gait is used less frequently than trotting or walking but can be beneficial for energy efficiency, terrain adaptability, and simplified control in certain conditions.However, the gait can lead to lateral instability, especially at higher speeds, unless the robot includes proper active balance control or inertial compensation.

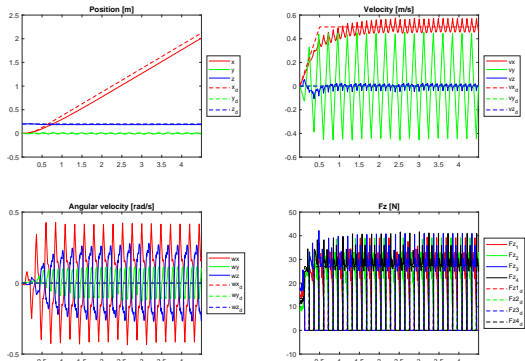


Figure 11: Pacing gait $m = 5.5\text{Kg}$ $\mu=1$ $v_{des} = [0.5;0]\text{m/s}$

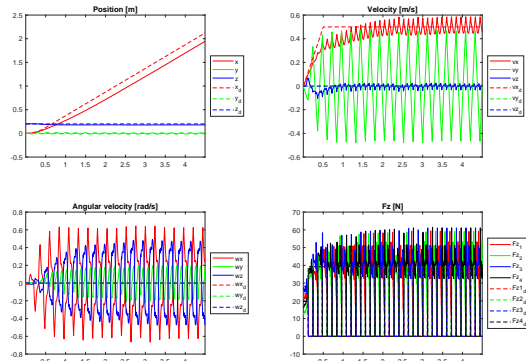


Figure 12: Pacing gait $m = 8\text{Kg}$ $\mu=1$ $v_{des} = [0.5;0]\text{m/s}$

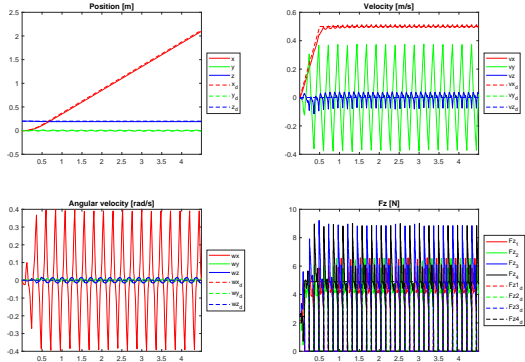


Figure 13: Pacing gait $m = 1\text{Kg}$ $\mu=1$ $v_{des} = [0.5;0]\text{m/s}$

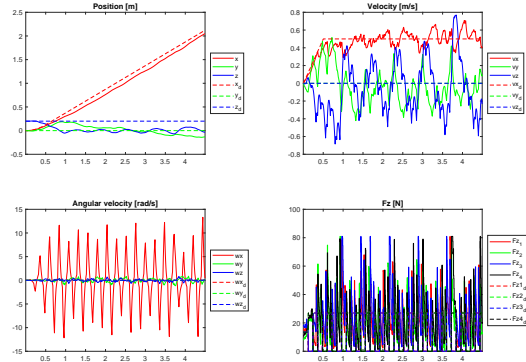


Figure 14: Pacing gait $m = 5.5\text{Kg}$ $\mu=0.4$ $v_{des} = [0.5;0]\text{m/s}$

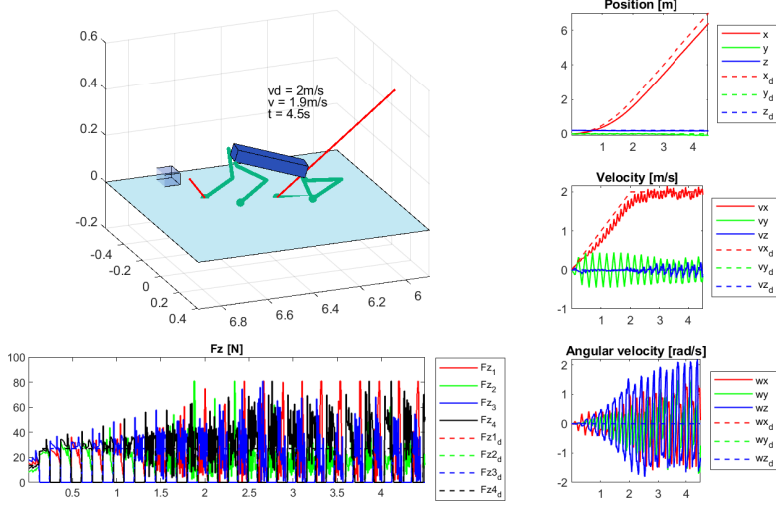


Figure 15: Pacing gait $m = 5.5\text{Kg}$ $\mu=1$ $v_{des} = [2;0]\text{m/s}$

Compared to the previous gait, this one demonstrates greater stability with a $m=5.5\text{ kg}, \mu=1$ and $v_{des} = [0.5;0]\text{m/s}$. It produces lower ground reaction forces, remaining below 40 N, and maintains an almost constant position tracking error. When the mass is reduced, the robot shows improved precision in its movements due to lower inertial forces, resulting in better position tracking and more manageable ground reaction forces, which drop to around 9 N. This change also contributes to enhanced overall stability. However, increasing the mass to 8 kg negatively affects performance, causing a rise in position tracking error and a significant decline in stability. Increasing the speed leads to higher tracking errors and a noticeable loss of stability. The ground reaction forces also become more impulsive, as the system struggles to respond and maintain balance. Furthermore, reducing the friction coefficient to 0.4 severely compromises the robot's ability to maintain its position, often resulting in slips and loss of control. This instability is visually confirmed by the robot tipping over completely.

Gallop gait: The gallop is the highest-speed gait, but it offers limited stability due to phases where only a single leg maintains ground contact. Simulations using standard parameters reveal increased instability and a higher position tracking error. Galloping also introduces greater impact forces and instability, making it less suitable for rough terrain.

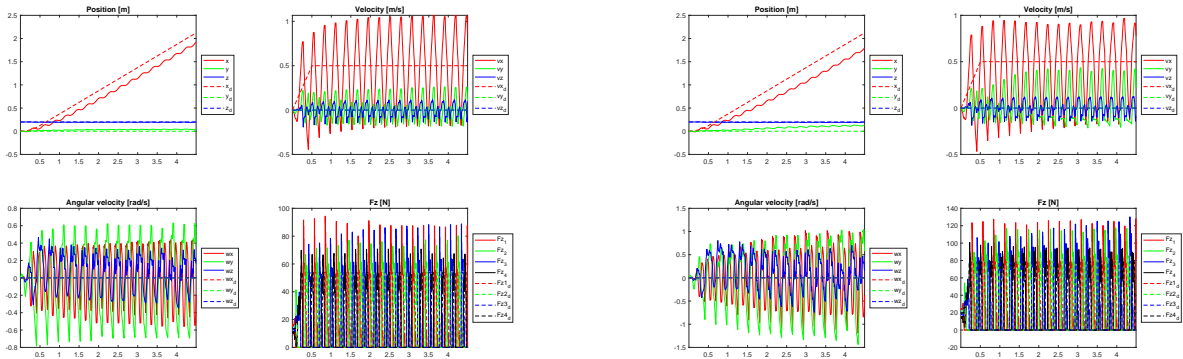


Figure 16: Gallop gait $m = 5.5\text{Kg}$ $\mu=1$ $v_{des} = [0.5;0]\text{m/s}$

Figure 17: Gallop gait $m = 8\text{Kg}$ $\mu=1$ $v_{des} = [0.5;0]\text{m/s}$

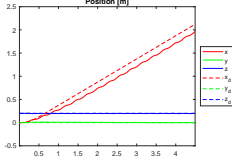


Figure 18: Gallop gait $m = 1\text{Kg}$ $\mu=1$ $v_{des} = [0.5;0]\text{m/s}$

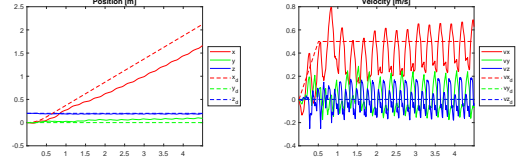
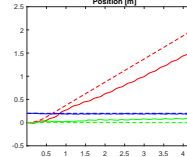
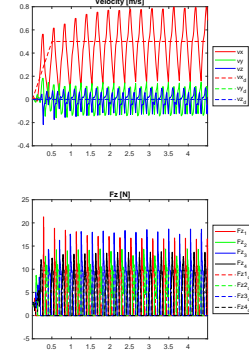


Figure 19: Gallop gait $m = 5.5\text{Kg}$ $\mu=0.4$ $v_{des} = [0.5;0]\text{m/s}$

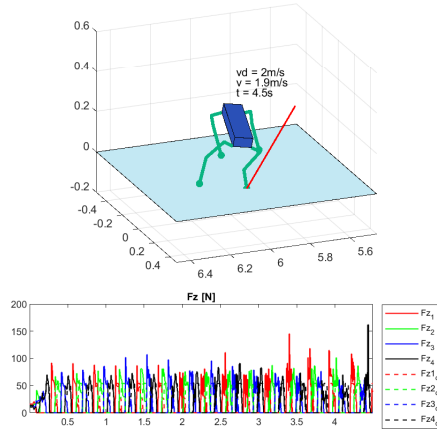
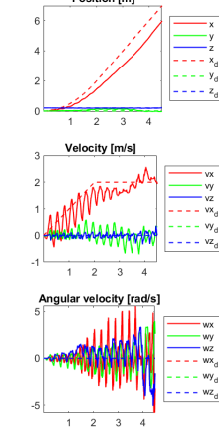


Figure 20: Gallop gait $m = 5.5\text{Kg}$ $\mu=1$ $v_{des} = [2;0]\text{m/s}$



Adjusting the mass shows that a slight reduction can offer marginal improvements in stability. When speed is increased, the gallop gait begins to break down—oscillations in the robot’s movement become more significant, disrupting its ability to follow a consistent path. At higher velocities, this gait shows clear signs of instability and unnatural behavior, as illustrated in the subsequent figures. Furthermore, lowering the coefficient of friction exacerbates these problems, introducing greater instability and increased oscillations. Under these conditions, the robot struggles to maintain its balance, frequently slipping and even falling. This is accompanied by a notable rise in position errors and a further decline in stability.

Trot-run: It maintains the diagonal limb coordination typical of a trot with shorter flight phases. This implies that, unlike the trot, the robot’s legs spend less time in the air. While this gait is more dynamic, it is also less stable, with increased risk of imbalance due to the shorter flight phases.

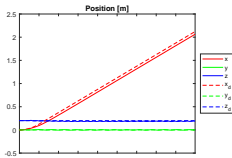


Figure 21: Trot run gait $m = 5.5\text{Kg}$ $\mu=1$ $v_{des} = [0.5;0]\text{m/s}$

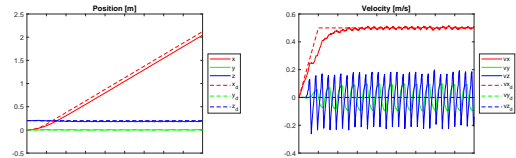
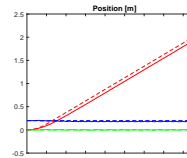
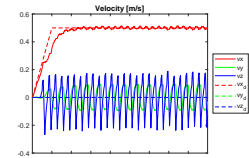


Figure 22: Trot run gait $m = 8\text{Kg}$ $\mu=1$ $v_{des} = [0.5;0]\text{m/s}$

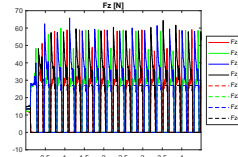
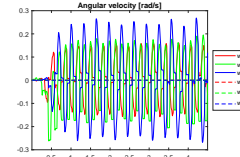
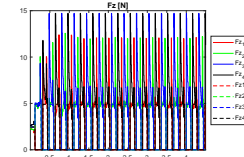
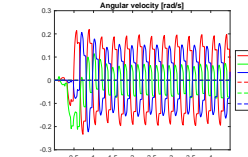
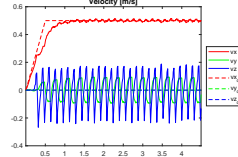
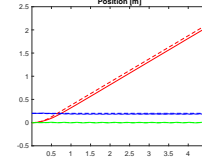
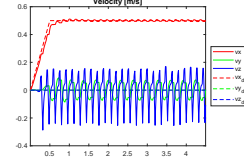
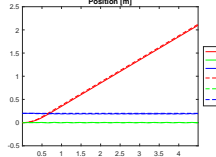


Figure 23: Trot run gait $m = 1\text{Kg}$ $\mu=1$ $v_{des} = [0.5;0]\text{m/s}$

Figure 24: Trot run gait $m = 5.5\text{Kg}$ $\mu=0.4$ $v_{des} = [0.5;0]\text{m/s}$

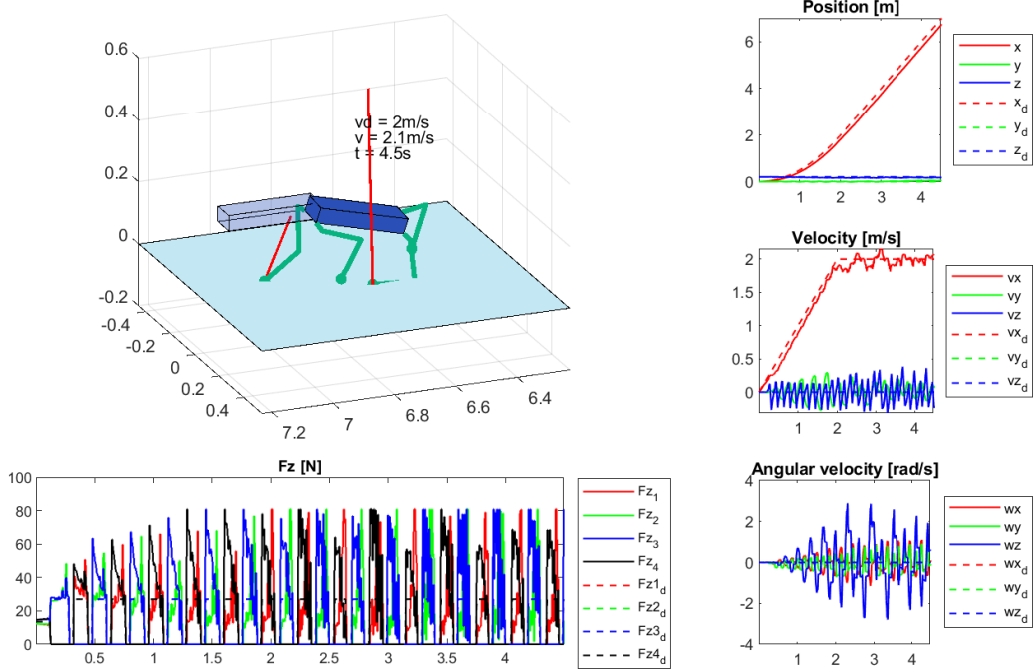


Figure 25: Trot run gait $m = 5.5\text{Kg}$ $\mu=1$ $v_{des} = [2;0]\text{m/s}$

Simulations with standard parameters immediately reveal that ground reaction forces peak at around 60 N approximately twice that observed in the trot gait—indicating increased mechanical stress during movement. The robot quickly reaches its target speed with minimal oscillations, and the position error remains relatively low. When the mass is reduced, there is a noticeable improvement in position tracking, and a slight enhancement in stability is observed; however, this adjustment alone is not sufficient to eliminate instability. Increasing the speed leads to more pronounced tracking errors, and the robot tends to drift away from its intended path, highlighting a reduction in overall stability. Additionally, lowering the friction coefficient results in even greater instability and an increase in tracking errors, as the robot struggles to maintain grip and control under such conditions.

Crawl Gait: is the slowest and most statically stable form of quadrupedal locomotion. It is characterized by the sequential movement of one limb at a time, with the other three limbs maintaining ground contact for support. This creates a "tripod" of stability at all times, making the crawl gait extremely robust against tipping or imbalance. This form of locomotion is the slowest among all the gaits considered in the analysis. This gait is frequently used during low-speed navigation, especially when a robot must move carefully over obstacles, stairs, or uneven terrain. The crawl gait offers maximum stability and reliability, it is also the least efficient in terms of speed and energy use.

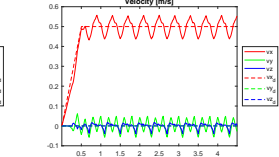
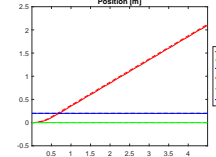
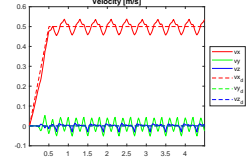
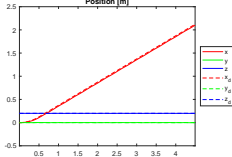


Figure 26: Crawl gait $m = 5.5\text{Kg}$ $\mu=1$ $v_{des} = [0.5;0]\text{m/s}$

Figure 27: Crawl gait $m = 8\text{Kg}$ $\mu=1$ $v_{des} = [0.5;0]\text{m/s}$

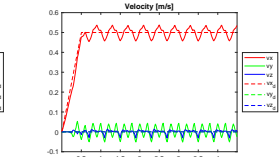
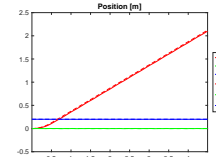
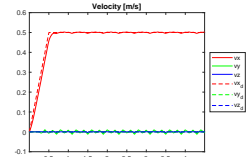
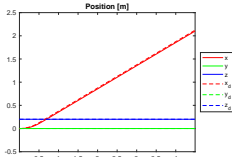


Figure 28: Crawl gait $m = 1\text{Kg}$ $\mu=1$ $v_{des} = [0.5;0]\text{m/s}$

Figure 29: Crawl gait $m = 5.5\text{Kg}$ $\mu=0.4$ $v_{des} = [0.5;0]\text{m/s}$

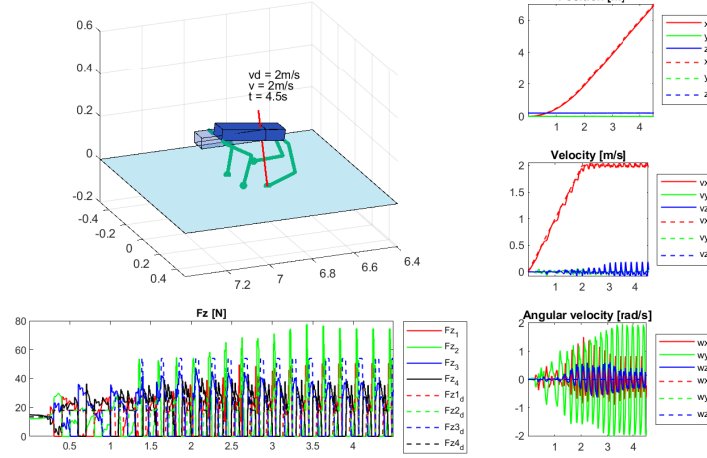


Figure 30: Crawl gait $m = 5.5\text{Kg}$ $\mu=1$ $v_{des} = [2;0]\text{m/s}$

Ground reaction forces peak at around 45 N, and position tracking errors are minimal, reflecting high precision. When the robot's mass is reduced, stability improves further, with enhanced control over its positioning. However, increasing the speed makes the gait more dynamic, which in turn reduces its inherent stability. The simulation results show that the Crawl gait maintains effective balance only at lower speeds. Lastly, decreasing the coefficient of friction negatively affects the robot's performance, leading to reduced tracking accuracy, delayed control responses, minor oscillations in angular velocities, and an overall loss of balance.

Quadruped robot gaits differ notably in terms of velocity, stability, and the intensity of ground reaction forces. Among the various gaits studied, the most dynamic are the bound and gallop, which enable the robot to achieve high speeds. However, these gaits come with a trade-off, as they exhibit reduced stability and are more susceptible to instability, particularly on surfaces with low friction. On the other end of the spectrum, the crawl and trot gaits stand out for their reliability and strong performance at lower speeds, offering a much higher degree of balance and control. Gaits such as trot and trot-run offer a compromise between speed and stability. The trot-run, in particular, allows for faster locomotion due to its shorter aerial phases, although it sacrifices some of the stability found in a traditional trot. The pacing gait represents a middle ground between the crawl and the trot, delivering moderate speeds with decent stability and manageable ground reaction forces. Importantly, a reduction in surface friction does not drastically impact the crawl and trot gaits, whereas more dynamic gaits like the bound experience challenges, and both the pacing and gallop gaits tend to fail under such conditions. Ultimately, selecting the most appropriate gait depends on the specific demands of the task, environmental conditions, and the desired balance between speed and control. While dynamic gaits are well-suited for quick movements on surfaces with good traction, more stable options like the trot or crawl are better suited for navigating uneven or low-friction terrains with precision and reliability.

4. Consider the MATLAB file `rimless_wheel.m`, which simulates the motion of a rimless wheel. You are required to:

- Modify the initial angular velocity (line 12) with both positive and negative values. Run the simulation, examine the time histories of the states and the resulting phase portrait, and provide a critical discussion of the observed behavior. For example, consider the following questions: To which equilibria does the system converge? How many distinct equilibria or limit cycles are present? Can you identify their respective basins of attraction?
- Modify the leg length (line 7), the inter-leg angle (line 8), and the slope inclination (line 9), while keeping the initial angular velocity fixed at 0.95 rad/s. Run the simulation and critically analyze the results. In particular, address questions such as: Which parameter changes affect the equilibrium conditions? Do these modifications result in different limit cycles compared to the previous case?

In the case of a positive initial angular velocity ($\dot{\theta}=0.95$ rad/s), the time evolution of the states θ and $\dot{\theta}$ shows initial oscillations that quickly decay, stabilizing after approximately 2.5 seconds. Specifically, θ settles around -0.3126 rad, while $\dot{\theta}$ converges to 0 rad/s, indicating that the system has reached a state of rest. When the initial angular velocity is negative ($\dot{\theta}=-0.95$ rad/s), a similar but mirrored behavior is observed: the states stabilize after about 2 seconds, with θ converging to 0.4726 rad and $\dot{\theta}$ again reaching 0 rad/s. In contrast to the cases with initial angular velocities of $\dot{\theta}_0 = \pm 0.95$ rad/s, where the system settles into a static equilibrium, a different behavior emerges when the initial angular velocity is set to $\dot{\theta}_0 = 1$ rad/s. As shown in the two figures 37-38, the time evolution of the states does not decay to zero, but instead settles into a sustained periodic oscillation. Specifically, the plot of θ and $\dot{\theta}$ over time reveals a repeating pattern that does not vanish, while the corresponding phase portrait clearly shows a closed trajectory in the state space. This indicates that the system does not reach a fixed point but rather converges to a stable limit cycle, characteristic of periodic walking behavior in the rimless wheel model.

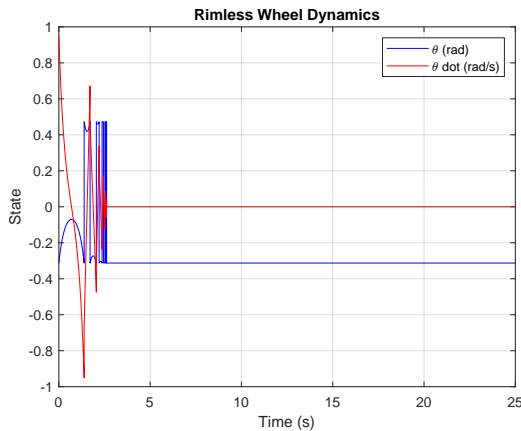


Figure 31: Rimless Wheel Dynamics with $\dot{\theta}_0=0.95$ rad/s

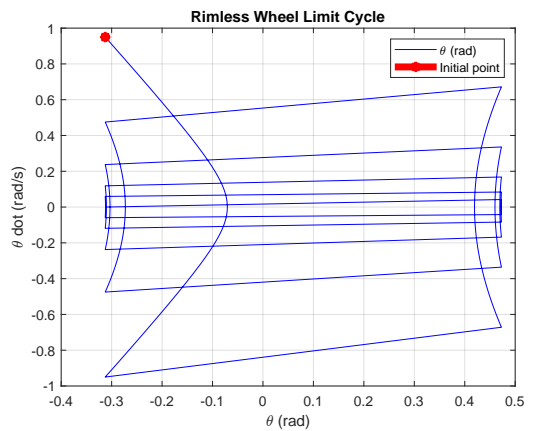


Figure 32: Rimless Wheel Dynamics with $\dot{\theta}_0=0.95$ rad/s

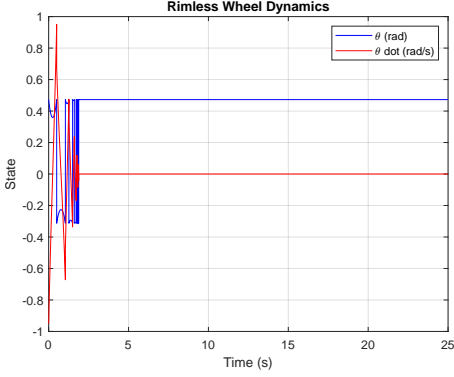


Figure 33: Rimless Wheel Dynamics with $\dot{\theta}_0 = -0.95 \text{ rad/s}$

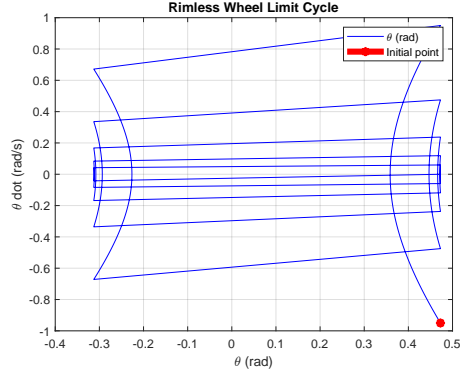


Figure 34: Rimless Wheel Limit Cycle with $\dot{\theta}_0 = -0.95 \text{ rad/s}$

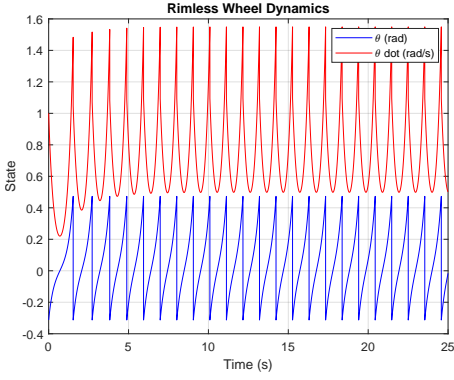


Figure 35: Rimless Wheel Dynamics with $\dot{\theta}_0 = 1 \text{ rad/s}$

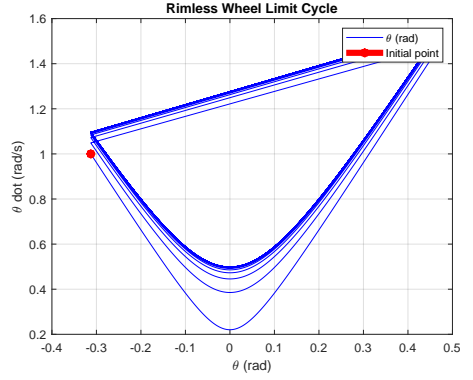


Figure 36: Rimless Wheel Limit Cycle with $\dot{\theta}_0 = 1 \text{ rad/s}$

The final state strongly depends on the initial conditions, particularly the sign of the angular velocity. Based on the numerical simulations, the system converges either to one of the two stable equilibria, θ_1 or θ_2 , or to a limit cycle, depending on the initial angular velocity $\dot{\theta}_0$. To classify the number of limit cycles, two key dynamical quantities were analyzed: the angular amplitude, defined as the difference between the maximum and minimum values of $\theta(t)$ over time, and the average period, computed as the mean time between the last few detected foot impacts. Trajectories identified as limit cycles were grouped using a relative tolerance-based clustering, where two cycles are considered equivalent if their amplitude and period differ by less than a fixed percentage. Using a 1% relative tolerance, the analysis revealed five distinct limit cycles, indicating that although the cycles exhibit nearly identical amplitudes, they differ slightly in their periods. It is worth noting that increasing the tolerance to 5% or 10% reduces the number of distinct limit cycles detected down to just one in some cases. This indicates that the differences found at tighter tolerances may arise from small numerical variations or transient dynamics, rather than representing fundamentally different attractors. As a result, the number of limit cycles ultimately depends on the precision used to define equivalence between periodic solutions.

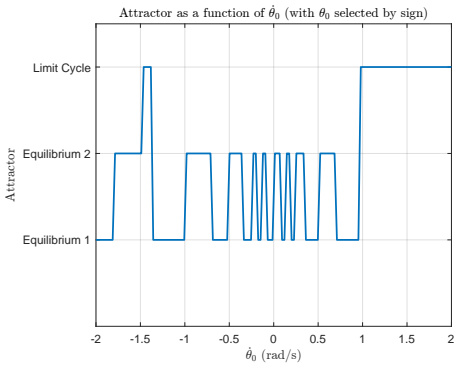


Figure 37: Basins of attraction for the 2 Equilibrium Points: Equilibrium 1=[-0.3126,0],Equilibrium 2=[0.4726,0]

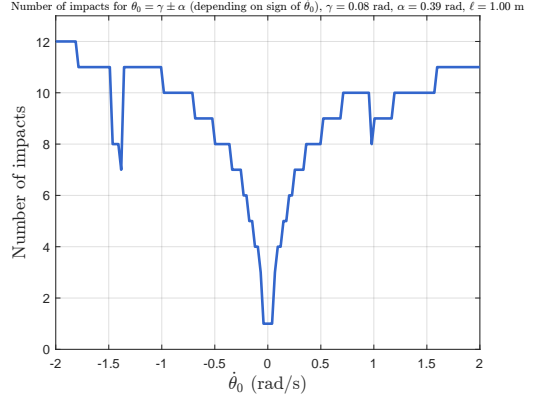


Figure 38: Number of impacts for θ fixed with : $\gamma = 0.08 \text{ rad}$, $\alpha = 0.39 \text{ rad}$, $\ell = 1.00 \text{ m}$

Figure 38, which reports the number of impacts before stabilization, provides additional insight into the system's dynamics. It can be observed that in the region corresponding to the limit cycle, the number of impacts is high and does not decay to zero, indicating that the system keeps stepping indefinitely. However, this data must be interpreted with caution: a high number of impacts does not necessarily imply the presence of a limit cycle.

A clear example is the case with $\dot{\theta}_0 = -2$ rad/s, where the system undergoes 12 impacts before coming to rest. Nevertheless, the time evolution of the states shows that the system reaches equilibrium quite rapidly: both θ and $\dot{\theta}$ settle within approximately 3.3 seconds. This suggests that the high number of impacts is due to large initial oscillations, rather than sustained periodic motion. Therefore, while the number of impacts can be a helpful indicator, it is only an indirect measure of the presence of a limit cycle and must be complemented by a qualitative analysis of the state trajectories.

Let us now see what happens when we modify the leg length, the inter-leg angle, and the slope inclination, while keeping the initial angular velocity constant at 0.95 rad/s. This helps us understand the influence of each parameter on the system's dynamics.

Effect of the slope angle γ on passive dynamics as α varies The slope angle plays a crucial role in enabling the rimless wheel to sustain periodic motion. For small values of γ , such as 0.04 rad, the gravitational potential energy introduced at each step is lower. As seen in Figure 39, the region in that supports limit cycle behavior is narrower than in cases with steeper slopes. In contrast, as γ increases to 0.08 rad and then to 0.12 rad (Figures 41 and 43), the energy added by the slope becomes sufficient to sustain walking for a much broader range of α . The basin of attraction widens, and the number of impacts before stabilization increases significantly (Figures 42 and 44), confirming more sustained motion. In particular, for $\gamma=0.12$ rad, the number of impacts peaks and remains high across a wide interval of α . The equilibrium points also shift with γ , chosen $\alpha = \pi/8$ rad and $l=1\text{m}$: for $\gamma = 0.04$ Equilibrium 1 = $[-0.3527; 0]$ Equilibrium 2 = $[0.4327; 0]$, for $\gamma=0.08$ Equilibrium 1 = $[-0.3126, 0]$ Equilibrium 2 = $[0.4726, 0]$ and for $\gamma=0.12$ Equilibrium 1 = $[-0.2727, 0]$ Equilibrium 2 = $[0.5127, 0]$.

Regarding the number of distinct limit cycles for the trajectories classified as limit cycles, a clustering procedure was applied using the same classification method described previously, where the parameter α was varied in the range $[2.8^\circ, 30^\circ]$. For $\gamma = 0.04$, the number of distinct limit cycles detected based on clustering in both period and amplitude was 179 with a 1% tolerance, 56 with 5%, and 32 with 10%. Similar results were obtained for $\gamma = 0.08$ and $\gamma = 0.12$. Unlike the analysis in which only the initial velocity $\dot{\theta}_0$ was varied, here the variation of α results not only in different periods but also in noticeable differences in oscillation amplitude, further supporting the classification of multiple distinct limit cycles.

The parameter α itself strongly influences gait characteristics. As shown in the basin of attraction, a small α results in short, frequent steps with minimal energy loss per impact, promoting stability and periodic walking. Conversely, a large α increases both step length and impact intensity.

Similar to γ , α also affects the equilibrium points: for instance, with $\dot{\theta}_0 = 0.95$ rad/s, $\gamma = 0.08$ rad, and $l = 1.00\text{m}$, Equilibrium 1 = $[-0.4436, 0]$ and Equilibrium 2 = $[0.6036, 0]$ for $\alpha = 0.52$ rad, and move to Equilibrium 1 = $[-0.1818, 0]$ and Equilibrium 2 = $[0.3418, 0]$ for $\alpha = 0.26$ rad.

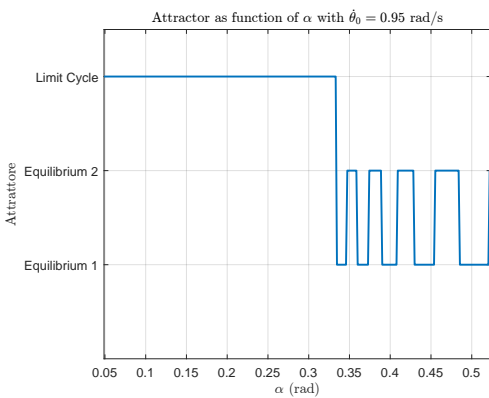


Figure 39: Attractor in function of α with $\dot{\theta}_0=0.95$ rad/s, $\gamma = 0.04$ rad, $l = 1.00\text{m}$, Equilibrium 1 (the negative) and Equilibrium 2 (the positive)

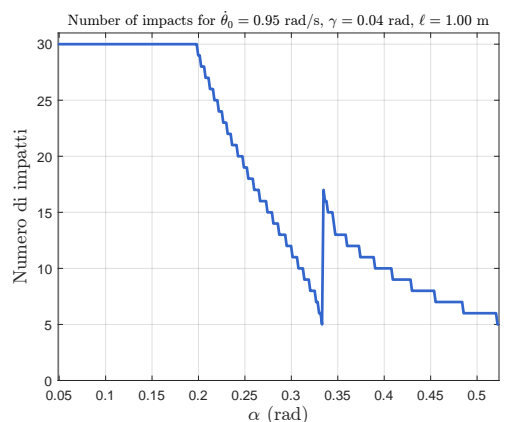


Figure 40: Number of impacts in function of α for $\dot{\theta}_0=0.95$ rad/s, $\gamma = 0.04$, $l = 1.00\text{m}$

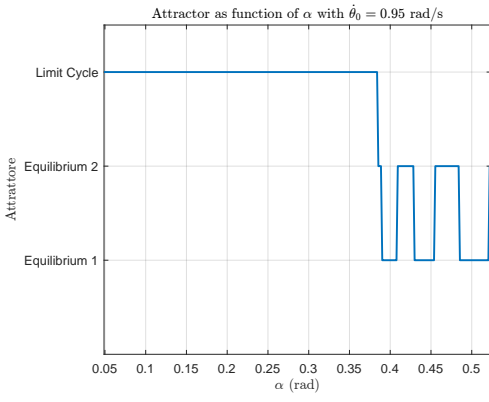


Figure 41: Attractor in function of α with $\dot{\theta}_0=0.95$ rad/s, $\gamma = 0.04$ rad, $\ell = 1.00$ m , Equilibrium 1 (the negative) and Equilibrium 2 (the positive)

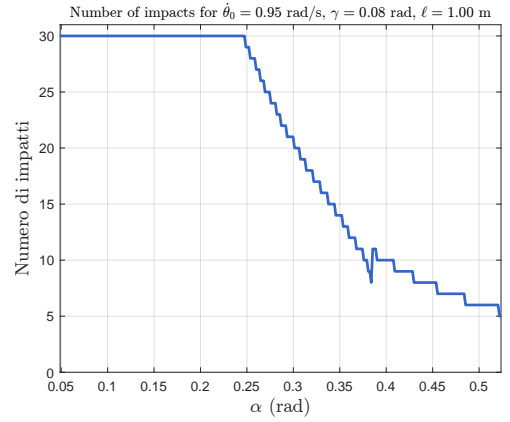


Figure 42: Number of impacts in function of α for $\dot{\theta}_0=0.95$ rad/s, $\gamma = 0.08$, $\ell = 1.00$ m

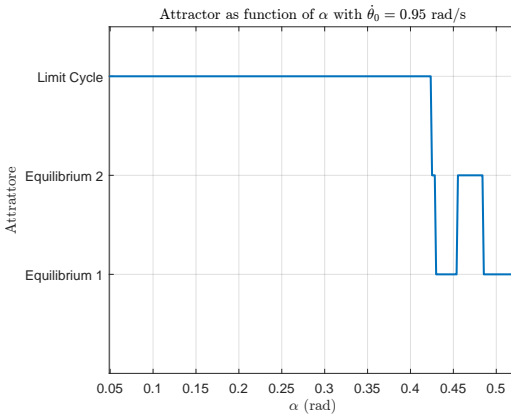


Figure 43: Attractor in function of α with $\dot{\theta}_0=0.95$ rad/s, $\gamma = 0.04$ rad, $\ell = 1.00$ m , Equilibrium 1 (the negative) and Equilibrium 2 (the positive)

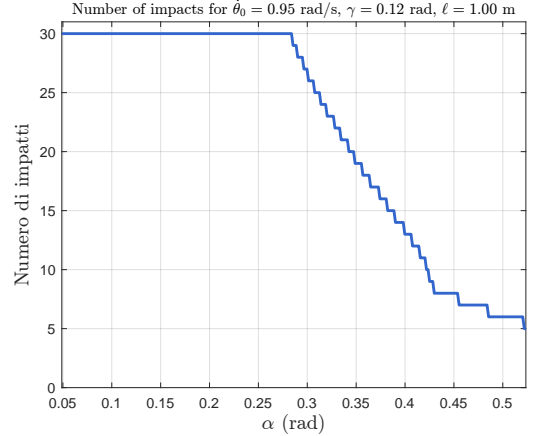


Figure 44: Number of impacts in function of α for $\dot{\theta}_0=0.95$ rad/s, $\gamma = 0.12$, $\ell = 1.00$ m

The leg length ℓ determines the arc traced by each step and the speed at which energy is dissipated or recovered. Shorter legs (e.g., $\ell = 0.5$ m) result in frequent impacts over small distances, which increases the cumulative energy loss and may lead the system to halt. Longer legs (e.g., $\ell = 1.5$ m), on the other hand, allow the wheel to cover more ground per step with smoother transitions, and the system benefits from a more efficient use of the gravitational potential gained from the slope.

Varying only the leg length ℓ does not affect the position of the equilibrium points, in this case with $\alpha = \pi/8$ and $\gamma = 0.08$ both with $\ell=1.5$ m and $\ell=0.5$ m the equilibrium points where Equilibrium 1 =[-0.3126;0] and Equilibrium 2=[0.4726;0].

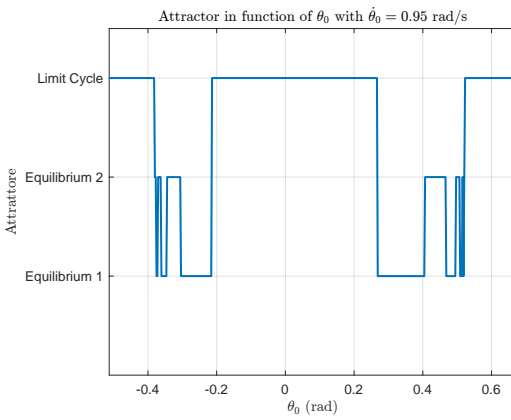


Figure 45: Attractor in function of θ_0 with $\dot{\theta}_0=0.95$ rad/s, $\gamma = 0.08$ rad, $\alpha = 0.39$ rad, $\ell = 0.50$ m , Equilibrium 1 (the negative) and Equilibrium 2 (the positive)

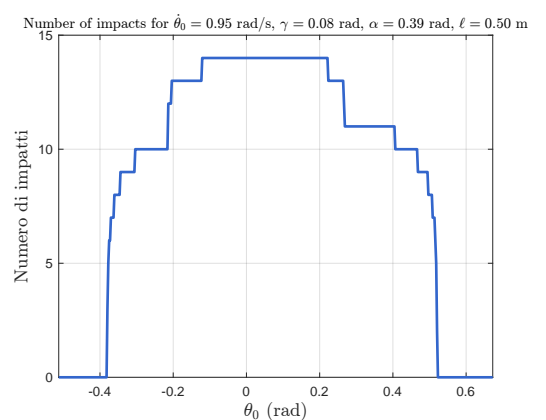


Figure 46: Number of impacts for $\dot{\theta}_0=0.95$ rad/s, $\gamma = 0.08$ rad, $\alpha = 0.39$ rad, $\ell = 0.50$ m

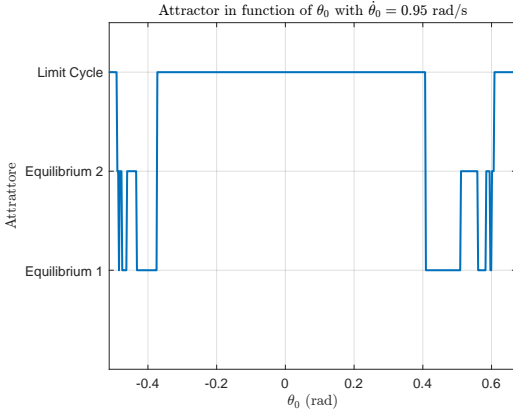


Figure 47: Attractor in function of θ_0 with $\dot{\theta}_0 = 0.95$ rad/s, $\gamma = 0.08$ rad, $\alpha = 0.39$ rad, $\ell = 1.50$ m , Equilibrium 1 (the negative) and Equilibrium 2 (the positive)

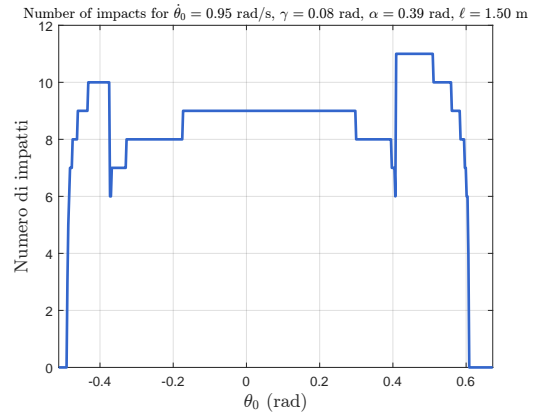


Figure 48: Number of impacts for $\dot{\theta}_0 = 0.95$ rad/s, $\gamma = 0.08$ rad, $\alpha = 0.39$ rad, $\ell = 1.50$ m

In this case, the trajectories classified as limit cycles were analyzed using the same criteria as in the previous section: both the amplitude and the period of oscillation were considered. For each leg length ℓ , distinct limit cycles were identified using relative tolerance thresholds of 1%, 5%, and 10%.

For $\ell = 1.5$ m, the number of distinct limit cycles was 14 with a 1% tolerance, 5 with a 5% tolerance, and 2 with a 10% tolerance. In contrast, for $\ell = 0.5$ m, the system consistently exhibited only 1 limit cycle across all tolerance levels (1%, 5%, and 10%).

It is worth noting that the variation observed among the different limit cycles was due solely to differences in their period, while the amplitude remained nearly constant across all cases.

In conclusion the behavior of the rimless wheel strongly depends on the initial angular velocity and system parameters. Positive and negative values of $\dot{\theta}_0$ lead to convergence toward two distinct stable equilibria, while higher magnitudes may produce limit cycles. Parameter changes such as slope γ and inter-leg angle α affect the position of equilibria and the emergence of limit cycles. In contrast, variations in leg length ℓ do not shift the equilibria.

In the scenario where only the initial angular velocity $\dot{\theta}_0$ was varied while keeping all physical parameters fixed, the system exhibited a family of limit cycles characterized by a nearly constant amplitude. In contrast, when physical parameters such as slope inclination γ , inter-leg angle α , and leg length ℓ were modified, the resulting limit cycles displayed clear variations in both amplitude and period. Increasing γ or α led to larger oscillation amplitudes and longer periods, as the system gained more potential energy per step or took larger angular strides. Changes in leg length ℓ , while not affecting the equilibrium positions, introduced a variety of limit cycles with different periods but relatively stable amplitude.